Understanding the Role of Elastic Modulus in the Relationship Between Second Harmonic Generation Scattering and Tumor Cell Motility

Tresa M. Elias
University of Rochester
Danielle Desa
University of Rochester
Phong Nguyen
University of Rochester
Ananya Goyal
University of Rochester
Danielle Benoit
University of Rochester
Mark R. Buckley
University of Rochester
Catherine K. Kuo
University of Rochester David and Ilene Flaum Eye Institute
Edward Brown (edward_brown@urmc.rochester.edu)
University of Rochester https://orcid.org/0000-0002-5367-5330

Research article

Keywords: Second Harmonic Generation, SHG, F/B ratio, collagen, metastasis

Posted Date: February 14th, 2020

DOI: https://doi.org/10.21203/rs.2.23511/v1

Abstract

Background: Second harmonic generation (SHG) is an intrinsic optical property of fibrillar collagen. SHG directionality is quantified by F/B, the ratio of forward- to backward-propagating signal, which is affected by collagen fiber internal structure, specifically the diameter, spacing, and disorder of fibrils within a collagen fiber. We have previously shown that F/B of primary invasive ductal carcinoma sections is prognostic of metastatic outcome. One possible cause of this relationship was revealed by our observation that tumor cells' motility on collagen I gels varied when collagen fiber internal structure in those gels was manipulated. The mechanism by which tumor cells sense changes in collagen fiber internal structure remains unknown: here we evaluate the role of elastic modulus in the relationship between collagen fiber internal structure (as reported by F/B) and tumor cell motility.

Methods: The 4T1 murine mammary adenocarcinoma, a model of metastatic triple negative breast cancer, (TNBC) and the 67NR line, a non-metastatic luminal phenotype, were introduced to a series of collagen-polyacrylamide mixed gels wherein collagen fiber internal structure and gel elastic modulus were independently controlled. F/B was measured with SHG, while elastic modulus was measured globally via rheometry and locally via atomic force microscopy (AFM). Tumor cell motility was quantified over three hours.

Results: The motility of both cell lines varied with F/B while elastic modulus was held constant, and did so at two physiological modulus values. Interestingly, 4T1 cell motility increased as F/B increased, while 67NR cell motility decreased.

Conclusions: Our results suggest that elastic modulus does not play a significant role in the observed relationship between collagen fiber internal structure (as reported by F/B) and tumor cell motility, for two cell lines that are models of TNBC and luminal-like breast cancer. Our observation that the two lines exhibit opposite motility trends as F/B increases is consistent with the trends in metastatic outcome versus F/B observed in our published clinical data for ER+ (i.e. containing the luminal subtypes) and ER- (i.e. containing the basal subtypes) cohorts, and suggests that a tumor's subtype may play a role in their response to collagen fiber internal structure.

1 Background

Breast cancer is one of the most common cancers with approximately 12.8% of women being diagnosed within their lifetime (1). Between 2009 and 2015, women diagnosed with localized, or stage 1, breast cancer had a 98.8% 5-year survival rate (1). However, women diagnosed with distant metastases had a significantly lower 5-year survival rate of 27.4% (1). Metastasis to a secondary location is an onerous journey for a cancer cell. Once the primary tumor is established, cells begin to migrate within their microenvironment and may reach a blood or lymphatic vessel. Once the cell reaches the vessel it can intravasate into the lumen and, if it survives, reach a distant organ where it may lodge and/or extravasate and possibly develop into a metastasis (2).

One of the earliest steps in the metastatic process is migration through the tumor extracellular matrix (ECM). The ECM is made up of various proteins including fibrillar collagen type I, which can be imaged with an intrinsic optical signal caused by the scattering phenomenon known as second-harmonic generation (SHG)(3–5). SHG is observed when two incoming photons scatter off a noncentrosymmetric structure to produce one photon at twice the energy and half the wavelength of the individual incoming photons. In tumors the only significant source of SHG signal is fibrillar collagen (6). SHG imaging has revealed that tumor cells can move along collagen fibers, and that the orientation of collagen fibers with respect to the border between breast tumor and host tissue can predict patient outcomes (7). This suggests that collagen fibers may act as 'roads' facilitating tumor cell escape from the primary tumor. When an excitation laser is focused on one point along an individual collagen fiber, SHG photons can scatter in the "forwards" direction, i.e. the direction of propagation of the laser, or in the "backwards" direction, i.e. in the opposite direction. This directionality can be quantified by collecting photons in both directions using two detectors and calculating the forwards-to-backwards scattering ratio, or "F/B". F/B is affected by properties of the internal structure of the collagen fiber including the diameter and spacing of the component fibrils that make up a fiber, as well as the order versus disorder in fibril packing (8–10). This internal structure is not the same as the direction of the fiber, but to extend the 'roads' analogy, F/B may provide information about road quality, as distinct from road direction.

Previously, we have shown that the F/B ratio of primary invasive ductal carcinoma (IDC) tumor biopsies is an independent prognostic indicator of patients' metastasis-free survival time in 10-year follow-up data (11). This suggests that F/B may be an additional indicator to assist in identifying which patients will metastasize and therefore who requires adjuvant chemotherapy. Hence the predictive ability of the F/B ratio of primary tumors may be useful in reducing the recognized clinical problem of "overtreatment"(12). To begin to understand why collagen fiber internal structure predicts metastatic outcome, in a previous study we determined the effect of varying collagen fiber internal structure on tumor cell motility in pure collagen gels (13). Collagen fiber internal structure was varied by varying gel polymerization conditions, and reported with F/B. We found that tumor cell motility was statistically significantly affected by varying collagen fiber internal structure (i.e. varying F/B) (13). This suggested that in patients, excised tumor F/B may be prognostic of metastatic outcome because the collagen fiber internal structure which dictates F/B also affects the efficiency with which cells escape the tumor. However, the underlying mechanisms of the relationship are still unidentified.

The elastic modulus of the extracellular matrix is known to have an impact on tumor cell behavior, including cell motility (14, 15). Therefore we hypothesized that cells could be reacting to modifications of collagen fiber internal structure because they are sensing matrix elastic modulus changes that may result from those modifications (15). To test this hypothesis, herein we characterized the motility of tumor cell lines in a series of collagen/polyacrylamide mixed gels in which we independently varied the collagen fiber internal structure and the elastic modulus (16–18). These gels provide an in vitro environment to study tumor cell motility and its relationship to ECM properties in the absence of other cellular actors, and their secreted factors, that may be present in an in vivo model. The two cell lines chosen were the metastatic 4T1 and nonmetastatic 67NR lines. The 4T1 murine mammary adenocarcinoma cells are a

common model of basal-like TNBC and were used in our previous studies (19, 20). For the non-metastatic cell line, 67NR was chosen since it is a paired sister cell line to the 4T1 cells (i.e. derived from the same tumor) and has a contrasting luminal phenotype(21, 22).

2 Methods

2.1 Multiphoton Image Acquisition

Multiphoton laser scanning microscopy (MPLSM) was conducted using a Ti:Sapphire excitation laser controlled through a BX61WI upright microscope (Olympus, Shinjuku, Tokyo), with beam scanning and image acquisition controlled by an Olympus Fluoview FV300 scanning system. The excitation light was circularly polarized with 100 fs pulses at 80 MHz. Circular polarization at the sample was achieved by passing the excitation light through a Berek compensator (Model 5540, New Focus, Irvine, CA) before entering the scan box. The light was focused through an Olympus UMPLFL20XW water immersion lens (20x, 0.95 N.A.), which was also used to collect the backwards scattered SHG signal. A 670 nm dichroic mirror was used to separate the backscattered signal from the excitation light. The backscattered SHG signal was filtered by a 405 nm band-pass filter (HQ405/30 m-2P, Chroma). Forward SHG signal was captured in the forward-scattered direction using an Olympus 0.9 N.A. optical condenser, reflected by a 565 nm long-pass dichroic mirror (565 DCSX, Chroma), and filtered by a 405 nm band-pass filter (HQ405/30 m-2P, Chroma). The SHG signal was generated with an excitation wavelength of 810 nm. All signals were captured by Hamamatsu HC125-02 photomultiplier tubes.

2.2 Cell Culture

The 4T1 mouse mammary adenocarcinoma cell line (Caliper Life Sciences, Hopkinton, MA) was frozen after three initial passages. Cells were maintained in a media consisting of RPMI (Gibco, Invitrogen Inc., Carlsbad, CA), 10% fetal bovine serum, and 1% penicillin/streptomycin. 67NR cells were purchased from the Animal Model & Therapeutic Evaluation Core (AMTEC) Barbara Karmanos Cancer Institute, Wayne State University. The 67NR cell line is a sister cell population to the 4T1 cell line, both derived from a single spontaneous Balb/cfC_3H. Cells were frozen after three initial passages. Cells were maintained in a media consisting of Dulbecco's Modified Eagle Medium (DMEM, Gibco 11965092), 10% fetal bovine serum, 1% 2 mM L-glutamine (Cellgro 25-005-Cl), and 0.1% 1 mM Mixed Nonessential Amino Acids (Gibco 11140).

2.3 Preparation of Collagen Polyacrylamide Mixed Gels

Mattek petri dishes (Ashland, MA) with 14-mm diameter coverslip-bottomed wells were coated with 2.5M NaOH and allowed to air dry. 200 µL of 97% 3-aminopropyltrimethoxy silane (APTES) was added to the coverslip bottom for 5 minutes and then rinsed three times with distilled water and gently dried with Kim Wipes. Each dish was flooded with 0.5% glutaraldehyde for 30 minutes and then rinsed three times with distilled water and allowed to air dry. Separate 12 mm glass coverslips were treated with RainX and allowed to air dry. Each coverslip was wiped to ensure an even coating and then sprayed again.

Collagen gels were made of human type I collagen solution at a concentration of 3 mg/mL (Advanced Biomatrix, San Diego, CA). With all solutions kept at 4 °C to minimize gelation, 810 µL of collagen type I was combined in a conical tube with 108 µL of RPMI 1640 media, and 50 µL of distilled water. The solution was vortexed at the lowest speed for 5 seconds to ensure the solution was evenly mixed. The pH of the solution was measured with a Mettler Toledo Micro Pro pH meter (Columbus, OH). The acceptable pH range for this solution was 7.5–7.7 (see below). In a petri dish, 6 droplets of 125 µL each of the solution was pipetted, making sure the droplets did not touch or spread and that all droplets were equal in size to ensure equal gelation. The petri dish was placed in an incubator for 2 hours at 37 °C and 5% CO_2.

Polyacrylamide is an easily manipulated polymer that can produce a wide range of elastic moduli, and when mixed with collagen will independently influence overall gel elastic modulus (16–18). Two polyacrylamide precursor solutions were made with different concentrations of acrylamide and bis-acrylamide. The first solution was 5% acrylamide: 0.1% bis-acrylamide and the second solution was 12% acrylamide: 0.25% bis-acrylamide; these combinations are known to produce polyacrylamide gels of significantly different elastic moduli (17). 375 µL of the desired polyacrylamide precursor was added to a conical tube. Once the collagen gel droplets gelled, they were added to the polyacrylamide precursor solution. This solution was vortexed on medium speed for 20 seconds to break up the collagen gels and mix thoroughly with the polyacrylamide. Next, 0.5 µL of N,N,N’,N’-tetramethylethylenediamine was added to the solution and followed by 5 µL of 10% w/v ammonium persulfate, for a final concentration of 0.5% and 5%, respectively; to minimize premature polymerization, this step was completed within 2 minutes. The solution was mixed by pipetting gently 10 times while avoiding bubbles. 100 µL of the solution was pipetted onto the center of the treated square coverslip, and then coverslipped with the treated circular coverslip. The solution was left at room temperature for 30 minutes to fully polymerize. This produces a final mixed gel with a uniform distribution of collagen fibers visible in SHG (Fig. 1) embedded within a polyacrylamide matrix.

The top coverslip was carefully removed with tweezers and the dish was washed with phosphate-buffered saline (PBS). The PBS was replaced with either RPMI or DMEM media, depending on which cells would be added to the gels. Gels were stored in the incubator overnight and subsequent experiments were performed within 24 hours.

2.4 Determining the F/B Ratio of Collagen Polyacrylamide Mixed Gels

During each imaging session, a standard fluorescein isothiocyanate (FITC) calibration sample was imaged with an excitation wavelength of 810 nm and 535 nm emission filters. Free FITC emits isotopically, which means the F/B ratio of a FITC calibration sample should be 1.0; any variation in the imaging system is reported by a variation in this measured ratio. To account for any day-to-day variation in the system, the background-subtracted SHG F/B ratios of the imaged samples on a given day (discussed below) are divided by the background-subtracted F/B ratio of the FITC calibration taken on

that day. For each image pair, an F and B image was taken with the laser shutter closed and the average pixel counts for each image provided the background.

For SHG F/B ratio analysis of the gels, two xyz stacks of simultaneously collected forward and backwards images were taken at a given xy region on the gel; three different regions of each gel were imaged. The forward and backward image pairs were taken at 50 μm steps through the depth of the gel. Each image was 660 μm x 660 μm.

ImageJ was used for all image analysis (23). The forward and backward images were background subtracted with the average background value for the corresponding direction. For each matched image pair, two masks of both the forward and the backward-scattered SHG signals were created, in which all collagen pixels were set to 1 and background pixels were set to 0 by applying a predetermined threshold to each of the two images. One forward threshold and one backward threshold was used for each imaging session and applied to all images. These thresholds were determined by surveying random background-subtracted images and adjusting the image's look-up tables until only collagen fibers are highlighted, and all other pixels were rejected. The two resultant masks for each matched image pair were then multiplied together to create a single mask that identifies pixels with SHG emission above the threshold in both the forward and backwards direction. A single F/B ratio image was calculated from the F and B image pair and then multiplied by the mask to set all non-fiber pixels to zero, thereby excluding these pixels from the analysis. The average pixel value of fiber pixels (i.e. non-zero pixels) for that region was then calculated for the masked F/B ratio image. This process was repeated in a for loop for each image pair in the stack for a single region. The average pixel value of each slice in the stack was then averaged to give a single F/B ratio for that region of the gel. The F/B ratio from all three regions were then averaged to produce a single F/B ratio to represent the entire gel.

To confirm that the measured F/B ratio was not affected by the thickness of the gel (i.e. that each gel was 'optically thin'), F/B was plotted as a function of imaging depth and a linear regression was performed. To exclude top and bottom edge effects, the middle 50% of the stack was used for analysis. Gels were only used if the slope of the line of best fit through the middle 50% of the stack was not significantly different from zero, thus ensuring that the measured F/B ratio was not affected by imaging depth.

2.5 Manipulation of F/B Ratio

The F/B ratio of the gels was altered by manipulating the pH of the collagen gel in the initial stage of making the mixed collagen-polyacrylamide gels as previously described (13). The pH was altered by using increasing amounts of 2.5M NaOH in the collagen gel solution to bring the final pH to 8.5–8.7 or 9.5–9.7, measured with a Mettler Toledo Micro Pro pH meter (Columbus, OH). The collagen gels were gelled and incorporated into the polyacrylamide as stated above. To verify that F/B varied with collagen gelation pH, the F/B of each gel was then plotted as a function the collagen pH during synthesis. A linear regression was performed to yield a p-value which would indicate whether the slope of the line of best fit was significantly different from zero or not.

2.6 Analysis of Tumor Cell Motility

The following preparation and imaging were performed one gel at a time. An hour prior to imaging, all media was removed from the gel and 1×10^4 cells were resuspended in their respective media and added to the surface of the gel in a droplet. The gel was placed in the incubator for an hour to allow the cells to adhere to the surface before all excess media was removed to minimize motion during the imaging session. Live cell images were taken on a Nikon Eclipse Ti microscope, using a Nikon MRH201201 air lens (20x, 0.45 N.A.). Cells were quickly transferred to a microscope stage incubator (Pathology Devices, Westminster, MD), at 37 °C, 5% CO_2, and 85% relative humidity. One phase contrast image was taken every 2 minutes for 3 hours and saved as a tiff file.

All image analysis was performed in ImageJ (23). For each gel, every cell in the field of view was tracked using the “Manual Tracking” ImageJ plugin, which tabulates the XY location of each cell at each time point (23). From this data, the total distance was calculated for each cell by summing the distance traveled between each time point. From this data, the five most motile and five least motile cells were identified and used for further analysis. To confirm that the gels did not significantly move during the imaging session, a fiducial artifact on each gel was identified and tracked in the same manner; total distance traveled by fiducial artifacts did not exceed 4.37 μm per imaging session and averaged 2.17 μm ± 1.62 μm, significantly less than the motion of all cells in all conditions. For comparison with previous literature (13), imaging sessions did not exceed three hours to ensure that there was no significant penetration of the cells into the gels and hence that the analysis remained two-dimensional.

2.7 Measuring Elastic Modulus with Atomic Force Microscopy

A silicon nitride tip probe with a radius of 20 nm and spring constant of 0.06 N/m (Bruker, CA, USA) was used on an MFP-3D AFM (Asylum Research, CA, USA) to obtain a 64 × 64 two-dimensional force map over a 20 μm x 20 μm area in the center of gels that were 600–700 μm thick. Elastic modulus measurements at each point on the force map were calculated by fitting force displacements curves to the Hertzian model, and force maps were averaged to yield a single elastic modulus measurement for each gel, as we previously described(24–27).

2.8 Measuring Elastic Modulus with Rheology

Global elastic modulus measurements of 8 mm diameter gels were performed using a parallel plate torsional rheometer (Discovery HR-2, TA Instruments). To prevent slippage, the gap distance between the rheometer plate and base was reduced in small steps (~ 10 ∝m) until the specimen was compressed with a constant axial force of -0.3 N. After compression, dynamic torsional shear mechanical tests were performed at an angular frequency of $\omega = 1$ rad/s across a range of strain amplitudes (0.01-1%). The shear storage modulus (G') was then computed at each strain level based on the measured time-dependent torque and angular displacement of the top plate. The value of G' for each gel was taken to be the average measurement of G' across all strain amplitudes. Assuming the gels were isotropic, the elastic modulus E was then determined according to $E = 3G'$.

3 Results

3.1 Development of Consistent Mixed Collagen/Polyacrylamide Gels that Maintain Optical Properties Necessary for MPLSM and Have Tunable Physical Properties

The methods described above produced mixed collagen/polyacrylamide gels with a uniform distribution of collagen fibers throughout (Fig. 1). To perform SHG imaging and obtain a single representative F/B value, the sample being imaged must be optically thin, which means that the measured F/B must not be affected by the imaging depth into the sample. When plotting F/B versus imaging depth, non-optically thin samples would have a slope significantly different than zero. The linear regression was only applied to the middle 50% of the image stack to exclude any edge effects. Thus, to confirm that the collagen polyacrylamide gels were optically thin, F/B was plotted against imaging depth and a linear regression was performed to determine the slope, as seen in Fig. 2. For each line, the p-value was much greater than 0.05, which indicates that F/B is not significantly affected by depth and the samples are optically thin. The gels used in this study were consistently ‘optically thin’.

3.2 Manipulation of F/B Ratio and Confirmation that F/B was Not Affected by Addition of Polyacrylamide

The F/B ratio of the gels was manipulated by altering the pH of the collagen gel during fibrillogenesis, and elastic modulus was manipulated by altering polyacrylamide polymerization, each as described above. The pH of the collagen was adjusted to either 7.5, 8.5 or 9.5. Figure 3 shows that F/B increases as pH of the collagen during synthesis increases, which is consistent with our previous studies (13). A two-way ANOVA was performed to compare the F/B of the high and low elastic modulus gels within a single pH category. A p-value greater than 0.05 and a Bonferroni post-hoc test revealed that there is no statistically significant difference between the F/B of the high and low modulus gels within a single pH category. Lastly, a t-test was performed to compare the slopes of the two lines in Fig. 3 which yielded a p-value much greater than 0.05, which indicates that the linear relationship between F/B and pH of collagen during synthesis is not affected by the presence of polyacrylamide nor its elastic modulus.

3.3 Evaluation of Elastic Modulus of Gels

The elastic modulus of the gels was manipulated by altering the acrylamide and bis-acrylamide concentrations in the polyacrylamide precursor solution. The ‘high modulus’ gels were composed of 12% acrylamide and 0.25% bis-acrylamide and the ‘low modulus’ gels were composed of 5% acrylamide and 0.1% bis-acrylamide. Figure 4a shows the elastic modulus of gels produced with these procedures, as measured by both AFM and rheology. At each modulus value, a two-way ANOVA was performed with Bonferroni post-hoc test to confirm that the AFM and rheology results were not statistically different.

Figure 4b shows the elastic modulus results from AFM plotted as a function of F/B. A linear regression for both data sets yielded a p-value greater than 0.05. The same analysis was performed for rheology data, with the same outcome (graph not shown). Taken together this data demonstrates that the mixed gels had an elastic modulus that could be tuned between two desired values (confirmed with both bulk rheology measurements as well as local AFM measurements), that the average values of elastic modulus were 1.738 ± 0.168 kPa and 18.504 ± 0.685 kPa (values that are relevant to tumor physiology (28)), and that alteration of collagen gelation did not affect the elastic modulus of the mixed gel.

3.4 4T1 and 67NR Cell Motility

Figures 5 and 6 shows the effect of varying collagen microstructure and elastic modulus on tumor cell motility of 4T1 cells and 67NR cells. For the most and least motile 4T1 cells, on the high and low modulus gels (Figures 5a and 5b), a linear regression fit of the total distance traveled versus F/B reveals that all four slopes have an F-test p-value <0.05, meaning that each slope is significantly different from zero. As the elastic modulus was held constant within each of the four combinations, this demonstrates that 4T1 cells can respond to variations in collagen fiber internal structure (as reported by F/B) independently of elastic modulus. The observation that motility of 4T1 cells increases with collagen gel F/B is consistent with our previous in vitro study (in which elastic modulus was not held constant) (13). Finally, cell motility was greater on gels of higher elastic modulus (2-way ANOVA, main effect of modulus $p < 0.0001$)(14, 15).

Figure 6a and 6b show the total distance traveled for 67NR cells on high and low modulus gels, respectively. For the most motile 67NR cells, on the high and low modulus gels, there is a significant relationship between the total distance traveled by the 67NR cells and F/B ($p = 0.0019$, $p = 0.0087$, linear regression), while elastic modulus was held constant. However, the least motile cells exhibit no significant relationship between total distance traveled and F/B on the high modulus gels ($p = 0.0827$, linear regression), but do exhibit a significant relationship on the low modulus gels ($p = 0.0283$, linear regression). Interestingly, the trend for the most motile 67NR cells is negative (i.e. the slope of the distance traveled versus F/B plot is negative), whereas the trend is positive for the 4T1 cells. Finally, cell motility was not significantly different between gels of lower versus higher elastic modulus (2-way ANOVA, main effect of modulus $p = 0.8583$)(14, 15).

4 Discussion

Previously, we have shown that the average F/B of primary IDC tumor biopsies is prognostic of metastatic outcome. Specifically, in ER + IDC tumors (i.e. including the luminal subtypes), patients whose tumors had higher F/B experienced fewer distant metastases in 10-year follow-up data (29, 30). Conversely, in ER^- IDC tumors (i.e. including the basal triple negative and HER2-enriched subtypes) the relationship was inverted and patients whose tumors had higher F/B experienced more distant metastases. One possible explanation for the prognostic relationship is provided by observations that tumor cells move along SHG-emitting collagen fibers in murine tumor models, and that the tendency of

those fibers to orient perpendicularly to the tumor/host interface in patient samples is prognostic of patient outcome (7). This suggests that collagen fiber internal structure (which dictates F/B) may influence the motility of tumor cells moving along a fiber and thereby alter the outflow of cells from a tumor, hence influencing metastatic outcome for the patient. Therefore, in previous work we examined the relationship between collagen fiber internal structure in pure collagen gels (as reported by F/B) and tumor cell motility of metastatic 4T1 cells, a model of basal-like triple negative breast cancer (TNBC), on those gels (13). We observed that motility increased as F/B of the collagen gels increased. That trend is consistent with the trend observed in the ER^- cohort in patient samples (containing basal TNBC patients), and those results suggest that in patient tumors F/B may predict metastasis because the collagen fiber internal structure upon which it depends influences the ability of tumor cells to locomote along those fibers and escape the tumor(13). However, the mechanisms by which tumor cells sense differences in collagen fiber internal structure, in order to respond with differences in motility, remains unclear.

One such mechanism is suggested by the ample literature demonstrating that elastic modulus of a cell's environment influences its behavior (14, 15). This suggests that cells may alter their motility by reacting to changes in elastic modulus that may result from changes in collagen fiber internal structure (15), or conversely that cells may directly sense changes in collagen fiber internal structure independently of elastic modulus. Therefore, herein we studied the role of elastic modulus in the relationship between collagen fiber internal structure, as reported by F/B, and tumor cell motility. To evaluate this relationship, we introduced metastatic and non-metastatic cell lines to mixed collagen/polyacrylamide gels of various F/B values and two different physiologically relevant values of elastic modulus. First, we created a series of in vitro gels with multiple values of F/B and elastic modulus. To develop these gels in our laboratory, we incorporated polyacrylamide into our previous pure collagen gel protocols (13). After developing this protocol, we first verified that the measured F/B was constant throughout each gel and was not affected by the presence of the polyacrylamide nor by variation of the elastic modulus (Fig. 3). Next, we confirmed that varying collagen fiber internal structure (as reported by F/B) by varying collagen polymerization conditions did not affect the measured elastic modulus and that all three F/B categories had the same elastic modulus (Fig. 4).

As demonstrated in Fig. 5a and 5b, in mixed collagen-polyacrylamide gels the motility of 4T1 cells increases as F/B of their microenvironment increases. These results confirm our previous study where we observed 4T1 motility increasing as F/B increased in pure collagen gels whose elastic modulus was not controlled (13). Furthermore, this specific trend of tumor cell motility increasing with F/B is consistent with the trend of metastasis-free survival time decreasing with F/B observed in patient tumor samples in the analogous (ER^-, containing basal TNBC) cohort of human patients. This suggests that F/B may predict metastatic outcome in patient samples because changing collagen fiber internal structure (which affects F/B) alters the outflow of cells from a tumor. Importantly, 4T1 motility increased with F/B even as the elastic modulus was held constant, as evidenced by both local AFM and global rheometry measurements (Fig. 5). This suggests that the 4T1 model of TNBC can respond to changes in internal collagen structure with changes in motility independently of significant changes in elastic modulus. In the

67NR model of luminal breast cancer we again observed that tumor cell motility varies with F/B and does so even as the elastic modulus was held constant (Fig. 6). This suggests that the 67NR model of luminal breast cancer can also respond to changes in internal collagen structure with changes in motility independently of significant changes in elastic modulus. Interestingly, we observe the opposite trend between motility and F/B in the 67NR cells versus 4T1 cells, as seen in Fig. 6a and 6b, where 67NR tumor cell motility decreases as F/B of the microenvironment increases. This is again consistent with the data from patient samples where metastasis-free survival time increases with increasing F/B in the ER + cohort, which contains the luminal subtypes (11). This again suggests that F/B may predict metastatic outcome in patient samples because changing collagen fiber internal structure (which affects F/B) alters the outflow of cells from a tumor. However it appears that the response of luminal-type breast tumor cells to alterations in collagen internal structure is opposite to the response of basal-type TNBC breast tumor cells (Figs. 5 and 6), although in both cases the response is not to changes in elastic modulus, but directly to changes in the collagen fiber internal structure.

This work also confirms observations in the literature that the motility of tumor cells varies when elastic modulus of their substrate is varied, and that different cell lines respond to changes in elastic modulus in different ways. At equivalent values of elastic modulus and F/B we observed that 4T1 cells were more motile than 67NR cells (Figs. 5 and 6). This is consistent with literature observations of their relative migration (31) and with the fact that unlike the highly metastatic 4T1 cells, 67NR cells very rarely metastasize to secondary locations and are typically unable to leave the primary site (21). At constant values of F/B the motility of 4T1 cells increase with elastic modulus while the motility of 67NR cells do not change (Figs. 5 and 6). This is consistent with literature observations of MDA-MB-231 (a model of basal TNBC cancer, analogous to 4T1s) and MCF7 (a model of luminal breast cancer, analogous to 67NRs) which exhibited the exact same behavior (i.e. increasing motility versus no change in motility) on substrates of similar elastic modulus (32).

5 Summary

To summarize, using a collagen/polyacrylamide gel system capable of independently varying collagen fiber internal structure and elastic modulus, we evaluated tumor cell motility under the influence of these two parameters. Our results suggest that variation in collagen fiber internal structure (as reported by F/B) can induce variation in tumor cell motility directly, independently of elastic modulus, in either a model of basal-like metastatic TNBC or a model of luminal-like non-metastatic breast cancer. Furthermore, we found that in the 67NR model of luminal breast cancer cell motility decreases as F/B increases, while in the 4T1 model of basal TNBC cell motility increases with F/B. This is consistent with observations of patient samples wherein luminal subtypes exhibited longer metastasis free survival (MFS) with increasing F/B while basal subtypes exhibited shorter MFS with increasing F/B (22). Taken together these results suggest that variations in collagen fiber internal structure do not modify tumor cell motility via any induced changes in elastic modulus. Furthermore, these results suggest that luminal and basal-type breast cancer reacts to changes in collagen fiber internal structure in different ways. In future work we hope to continue to explore the mechanism by which tumor cells sense changes in collagen fiber internal

structure. Our observation that these cells are not sensing changes in collagen fiber internal structure through elastic modulus suggests that there may be cell surface receptors that are directly sensitive to variations in this property. Furthermore, these fiber internal structure sensors may be different on basal versus luminal subtypes or may be linked to different signaling pathways.

Abbreviations

SHG:Second Harmonic Generation, F/B:Forward-to-backwards ratio, IDC:Invasive Ductal Carcinoma, ER+:Estrogen Receptor positive, ER-:Estrogen Receptor negative, ECM:Extracellular Matrix, MPLSM:Multiphoton Laser Scanning Microscopy, PBS:Phosphate Buffer Saline, FITC:Fluorescein Isothiocyanate, AFM:Atomic Force Microscopy, MFS:Metastasis-free Survival

Declarations

Ethics approval and consent to participate

Not applicable

Consent for publication

Not applicable

Availability of data and materials

The datasets used and/or analyzed during the current study are available from the corresponding author on reasonable request

Competing interests

The authors declare that they have no competing interests

Funding

This work was funded by Department of Defense Breast Cancer Research Program grant W81XWH-17-1-0011 and National Institutes of Health National Cancer Institute grant R21CA208921 to EB, Department of Defense Breast Cancer Research Program grant W81XWH-17-1-0015 to CKK, and a Wilmot Cancer Institute grant and a Breast Cancer Coalition of Rochester predoctoral traineeship to DD. The funding bodies had no role in in the design of the study, data collection, data analysis, data interpretation of data, nor in writing the manuscript.

Authors' Contributions

TE designed the protocol for collagen-polyacrylamide gels in consultation with PN and CKK, and prepared all gels for experiments, imaged and analyzed F/B data from all gels, performed cell motility experiments, and completed statistical analyses. TE is responsible for writing the majority of the manuscript. DD

contributed to the design of the experiment as well as data interpretation and troubleshooting. AG performed all rheometer measurements, as well as analyzed elastic modulus data. PN performed all AFM elastic modulus measurements and contributed to AFM analysis. CK provided consultation on making collagen-PA gels, access to AFM, as well as expertise and advice involving AFM and motility results. DB provided access to live cell imaging microscope, cell culture hoods, and incubators. MB provided access to rheometer as well as expertise in analyzing and comparing elastic modulus results. EB contributed to the design of the experiments, troubleshooting, data interpretation, and writing the manuscript.

All authors read and approved the final manuscript.

Acknowledgements

Not Applicable

Authors' Information

Not Applicable

References

1. National Cancer Institute Surveillance E, and End Results Program. Cancer Stat Facts: Female Breast Cancer: National Cancer Institute; 2019 [cited 2019 November 10th]. Available from: https://seer.cancer.gov/statfacts/html/breast.html.
2. Jin X, Mu P. Targeting Breast Cancer Metastasis. Breast Cancer (Auckl). 2015;9(Suppl 1):23-34.
3. Zoumi A, Yeh A, Tromberg BJ. Imaging cells and extracellular matrix in vivo by using second-harmonic generation and two-photon excited fluorescence. Proc Natl Acad Sci U S A. 2002;99(17):11014-9.
4. Campagnola PJ, Millard AC, Terasaki M, Hoppe PE, Malone CJ, Mohler WA. Three-dimensional high-resolution second-harmonic generation imaging of endogenous structural proteins in biological tissues. Biophys J. 2002;82(1 Pt 1):493-508.
5. Freund I, Deutsch M, Sprecher A. Connective tissue polarity. Optical second-harmonic microscopy, crossed-beam summation, and small-angle scattering in rat-tail tendon. Biophys J. 1986;50(4):693-712.
6. Brown E, McKee T, diTomaso E, Pluen A, Seed B, Boucher Y, et al. Dynamic imaging of collagen and its modulation in tumors in vivo using second-harmonic generation. Nat Med. 2003;9(6):796-800.
7. Conklin MW, Eickhoff JC, Riching KM, Pehlke CA, Eliceiri KW, Provenzano PP, et al. Aligned collagen is a prognostic signature for survival in human breast carcinoma. Am J Pathol. 2011;178(3):1221-32.
8. Han X, Burke RM, Zettel ML, Tang P, Brown EB. Second harmonic properties of tumor collagen: determining the structural relationship between reactive stroma and healthy stroma. Optics express. 2008;16(3):1846-59.

9. Williams RM, Zipfel WR, Webb WW. Interpreting second-harmonic generation images of collagen I fibrils. Biophys J. 2005;88(2):1377-86.
10. Lacomb R, Nadiarnykh O, Townsend SS, Campagnola PJ. Phase Matching considerations in Second Harmonic Generation from tissues: Effects on emission directionality, conversion efficiency and observed morphology. Optics communications. 2008;281(7):1823-32.
11. Burke K, Smid M, Dawes RP, Timmermans MA, Salzman P, van Deurzen CH, et al. Using second harmonic generation to predict patient outcome in solid tumors. BMC cancer. 2015;15:929.
12. Weigelt B, Peterse JL, van 't Veer LJ. Breast cancer metastasis: markers and models. Nature reviews Cancer. 2005;5(8):591-602.
13. Burke KA, Dawes RP, Cheema MK, Van Hove A, Benoit DS, Perry SW, et al. Second-harmonic generation scattering directionality predicts tumor cell motility in collagen gels. Journal of biomedical optics. 2015;20(5):051024.
14. Kraning-Rush CM, Reinhart-King CA. Controlling matrix stiffness and topography for the study of tumor cell migration. Cell Adh Migr. 2012;6(3):274-9.
15. Lo CM, Wang HB, Dembo M, Wang YL. Cell movement is guided by the rigidity of the substrate. Biophys J. 2000;79(1):144-52.
16. Wang YL, Pelham RJ, Jr. Preparation of a flexible, porous polyacrylamide substrate for mechanical studies of cultured cells. Methods Enzymol. 1998;298:489-96.
17. Syed S, Karadaghy A, Zustiak S. Simple polyacrylamide-based multiwell stiffness assay for the study of stiffness-dependent cell responses. J Vis Exp. 2015(97).
18. Baek K, Clay NE, Qin EC, Sullivan KM, Kim DH, Kong H. In situ assembly of the collagen–polyacrylamide interpenetrating network hydrogel: Enabling decoupled control of stiffness and degree of swelling. European Polymer Journal. 2015;72:413-22.
19. Martin JL, Julovi SM, Lin MZ, de Silva HC, Boyle FM, Baxter RC. Inhibition of basal-like breast cancer growth by FTY720 in combination with epidermal growth factor receptor kinase blockade. Breast Cancer Res. 2017;19(1):90.
20. Ghosh A, Sarkar S, Banerjee S, Behbod F, Tawfik O, McGregor D, et al. MIND model for triple-negative breast cancer in syngeneic mice for quick and sequential progression analysis of lung metastasis. PLoS One. 2018;13(5):e0198143.
21. Aslakson CJ, Miller FR. Selective events in the metastatic process defined by analysis of the sequential dissemination of subpopulations of a mouse mammary tumor. Cancer Res. 1992;52(6):1399-405.
22. Johnstone CN, Smith YE, Cao Y, Burrows AD, Cross RS, Ling X, et al. Functional and molecular characterisation of EO771.LMB tumours, a new C57BL/6-mouse-derived model of spontaneously metastatic mammary cancer. Dis Model Mech. 2015;8(3):237-51.
23. Rueden CT, Schindelin J, Hiner MC, DeZonia BE, Walter AE, Arena ET, et al. ImageJ2: ImageJ for the next generation of scientific image data. BMC Bioinformatics. 2017;18(1):529.

24. Pan XS, Li J, Brown EB, Kuo CK. Embryo movements regulate tendon mechanical property development. Philosophical transactions of the Royal Society of London Series B, Biological sciences. 2018;373(1759).
25. Marturano JE, Schiele NR, Schiller ZA, Galassi TV, Stoppato M, Kuo CK. Embryonically inspired scaffolds regulate tenogenically differentiating cells. J Biomech. 2016;49(14):3281-8.
26. Schiele NR, von Flotow F, Tochka ZL, Hockaday LA, Marturano JE, Thibodeau JJ, et al. Actin cytoskeleton contributes to the elastic modulus of embryonic tendon during early development. J Orthop Res. 2015;33(6):874-81.
27. Marturano JE, Arena JD, Schiller ZA, Georgakoudi I, Kuo CK. Characterization of mechanical and biochemical properties of developing embryonic tendon. Proc Natl Acad Sci U S A. 2013;110(16):6370-5.
28. Plodinec M, Loparic M, Monnier CA, Obermann EC, Zanetti-Dallenbach R, Oertle P, et al. The nanomechanical signature of breast cancer. Nat Nanotechnol. 2012;7(11):757-65.
29. Burke K, Tang P, Brown E. Second harmonic generation reveals matrix alterations during breast tumor progression. J Biomed Opt. 2013;18(3):31106.
30. Norum JH, Andersen K, Sorlie T. Lessons learned from the intrinsic subtypes of breast cancer in the quest for precision therapy. Br J Surg. 2014;101(8):925-38.
31. Eckhardt BL, Parker BS, van Laar RK, Restall CM, Natoli AL, Tavaria MD, et al. Genomic analysis of a spontaneous model of breast cancer metastasis to bone reveals a role for the extracellular matrix. Mol Cancer Res. 2005;3(1):1-13.
32. Ansardamavandi A, Tafazzoli-Shadpour M, Shokrgozar MA. Behavioral remodeling of normal and cancerous epithelial cell lines with differing invasion potential induced by substrate elastic modulus. Cell Adh Migr. 2018;12(5):472-88.

Figures

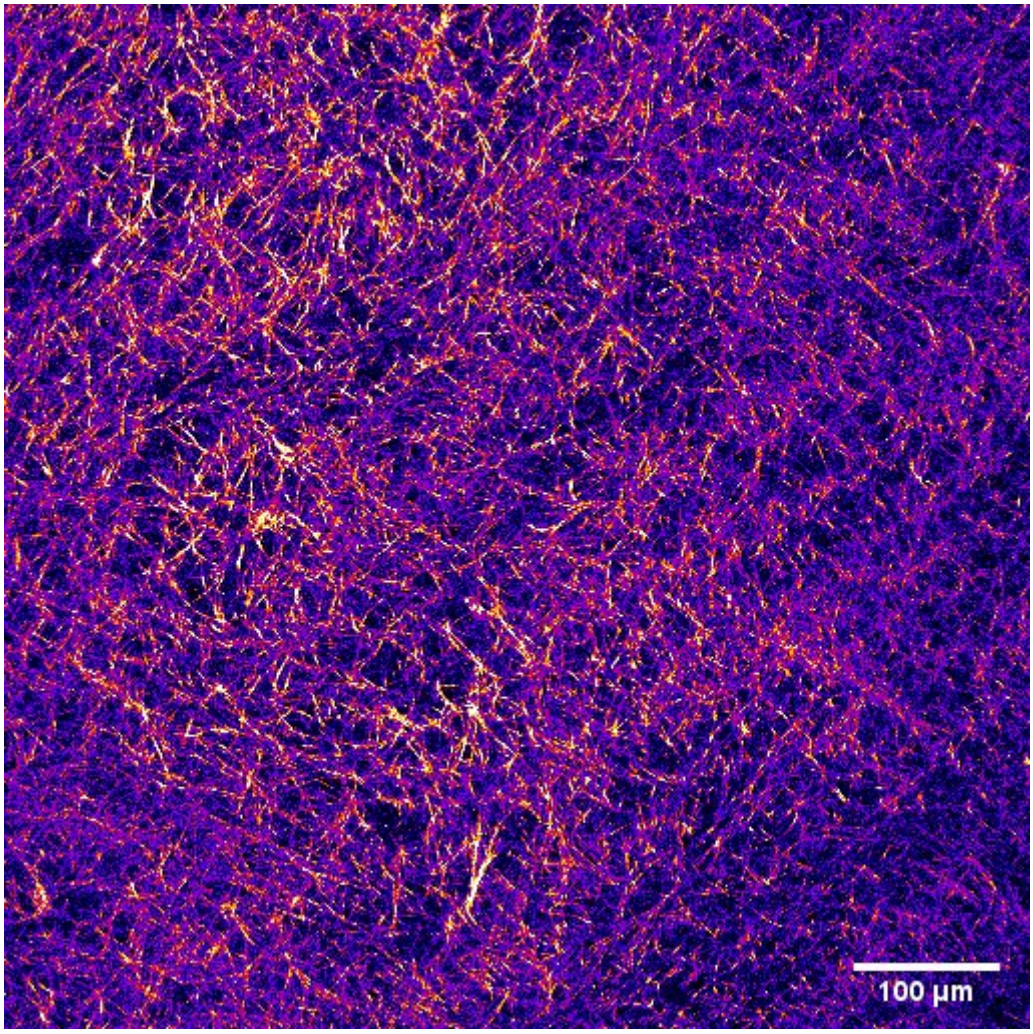

Figure 1

Representative background-subtracted forward-scattered SHG image of a mixed collagen/PA gel.

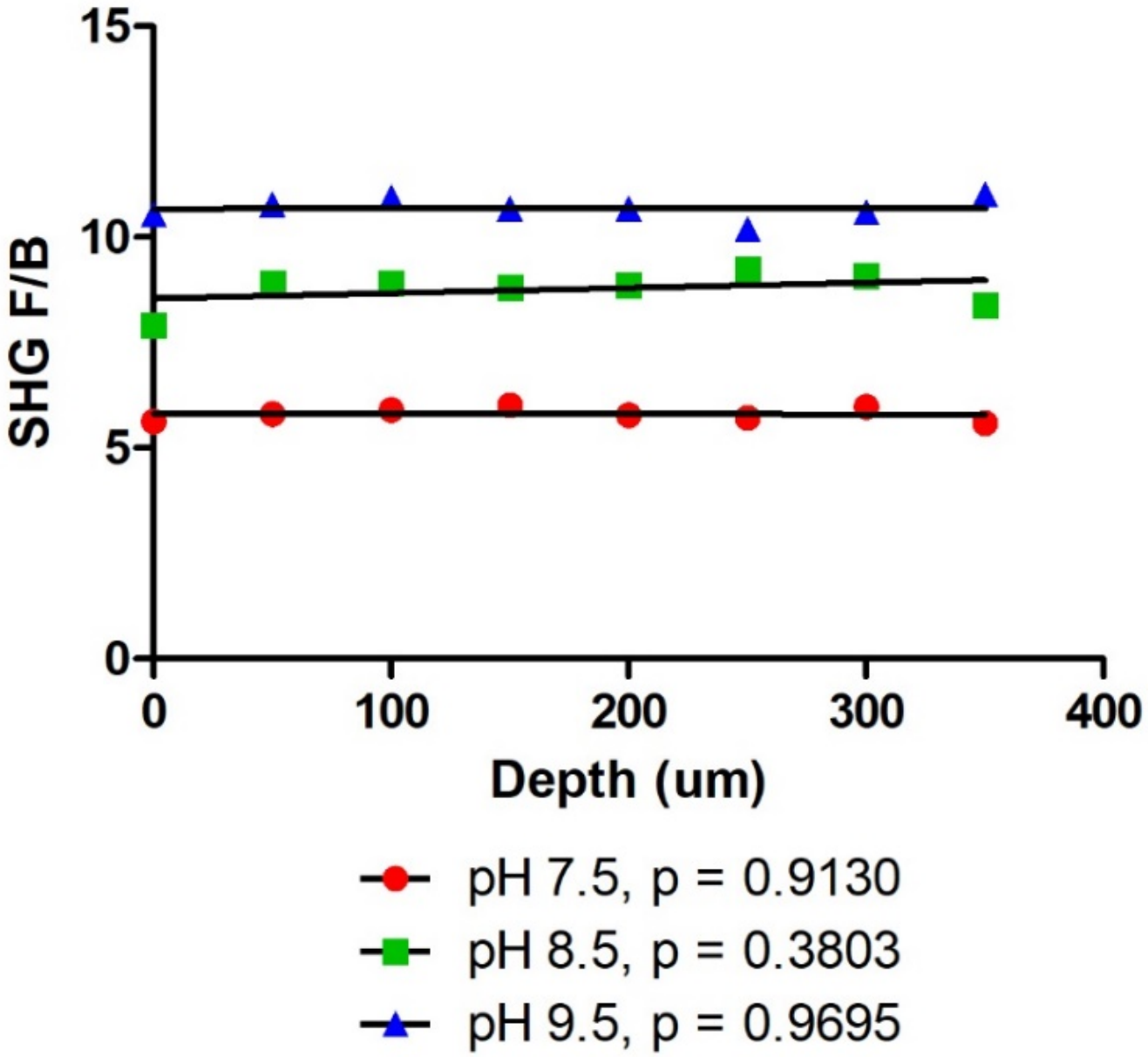

Figure 2

SHG F/B plotted versus imaging depth with corresponding linear regression p-values. Each line represents a single region of a single gel. Edge effects are not shown as only the middle 50% of each image stack is plotted.

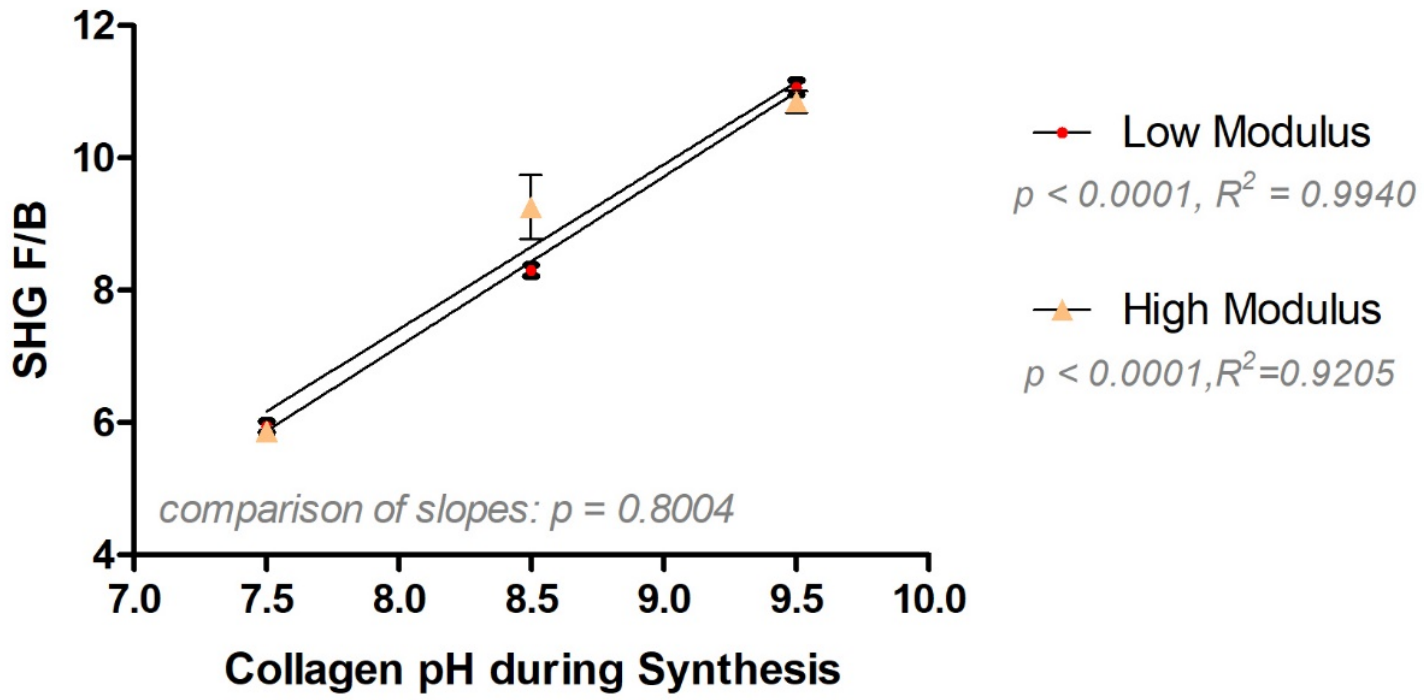

Figure 3

Relationship between SHG F/B and collagen pH during synthesis. Each point represents n=3 gels where each gel value is an average of the F/B of three different regions of that gel. A linear regression yielded p < 0.0001 for both the high and low modulus data. A Pearson's correlation test yielded R2 values of 0.9940 and 0.9205 for the low and high modulus gels, respectively. A t-test comparing the slopes of the two lines yielded p = 0.8004. Data shown as averages ± SEM.

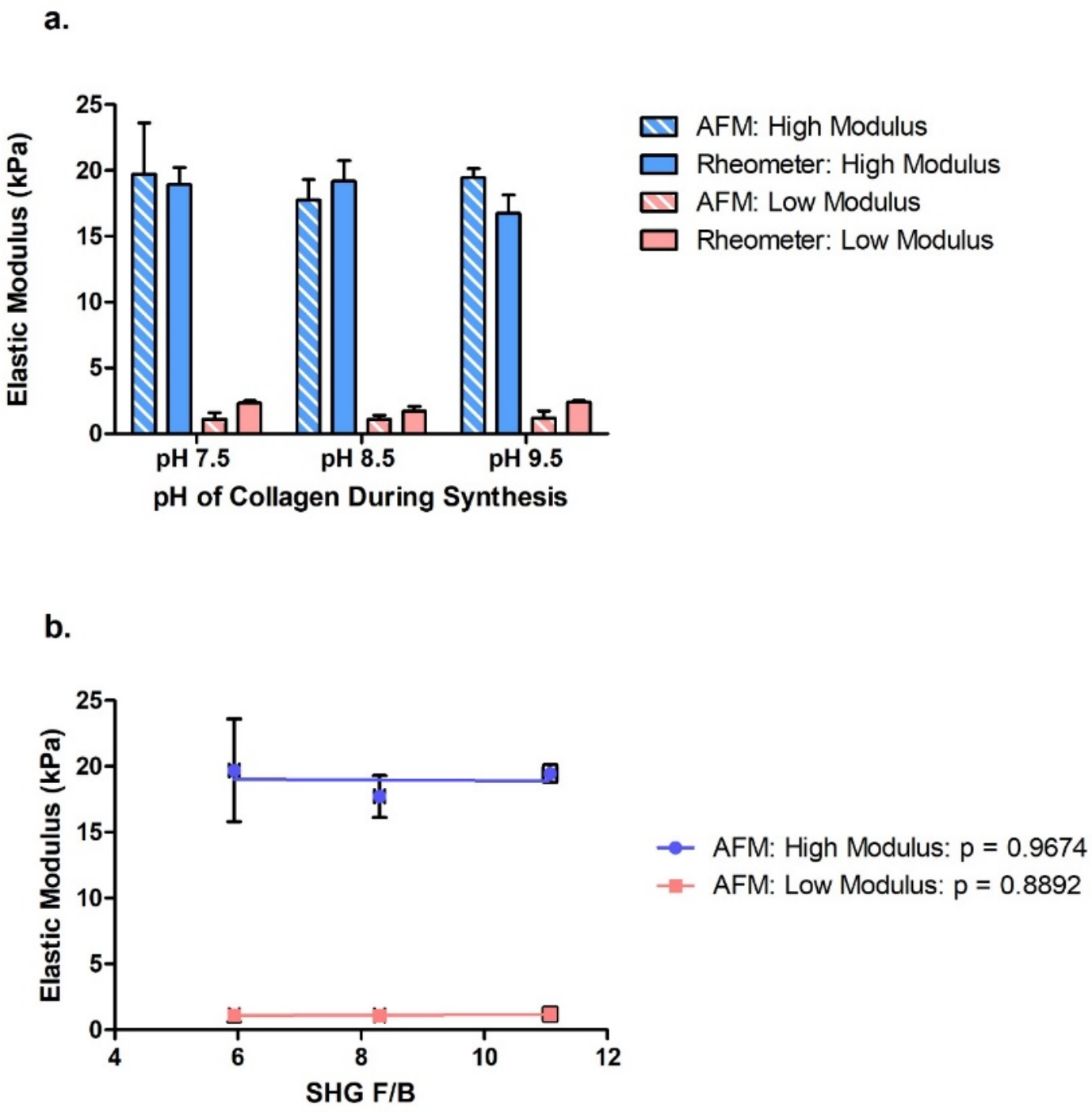

Figure 4

(a) AFM (n=3) and rheometer (n=5) results of 'high' and 'low' modulus gels of various synthesis conditions (yielding different collagen fiber internal structures). A one-way ANOVA comparing the two measurements at each modulus (comparing blue stripes to solid blue and red stripes to solid red) yielded $p > 0.05$, indicating that the two measurements produced statistically similar results. Data shown as averages ± SEM. (b) Elastic modulus as a function of F/B for high and low modulus data: linear regression $p > 0.05$ (n=3).

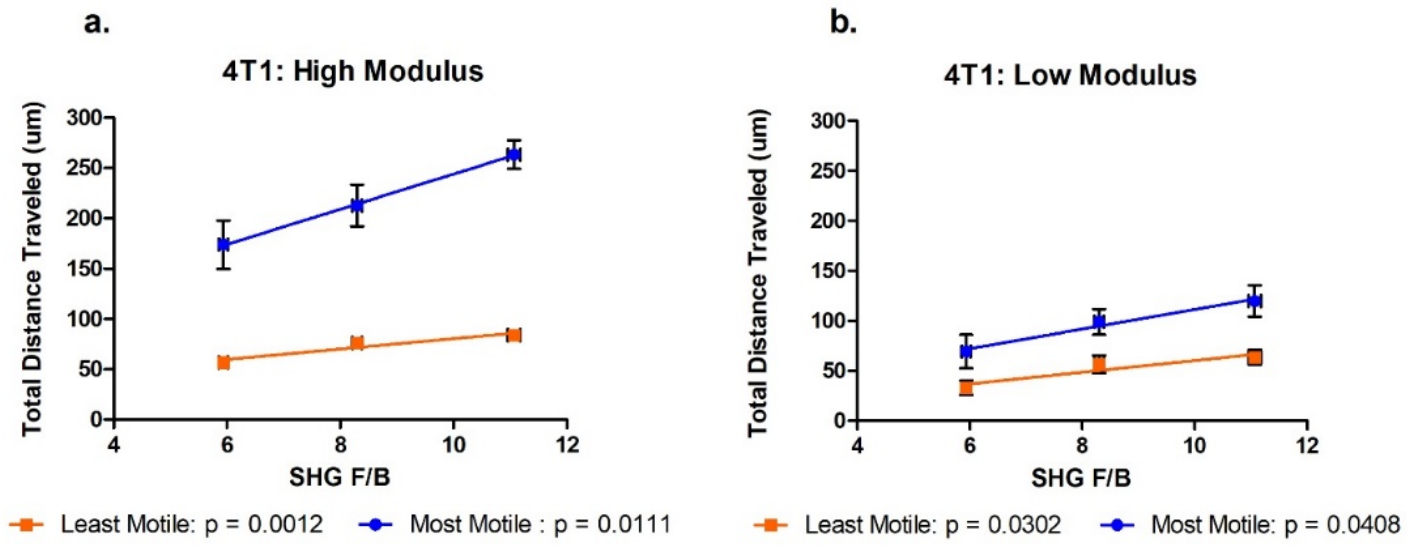

Figure 5

Effect of collagen fiber internal structure, as reported by F/B, and elastic modulus on tumor cell motility of metastatic 4T1 cells. Data shown as averages ± SEM (n = 3 gels). (a) Total distance traveled of the most and least motile 4T1 cells on high modulus gels of various F/B. (b) Total distance traveled of the most and least motile 4T1 cells on low modulus gels of various F/B. Stated p values represent the differences between linear regression slopes and a slope of zero.

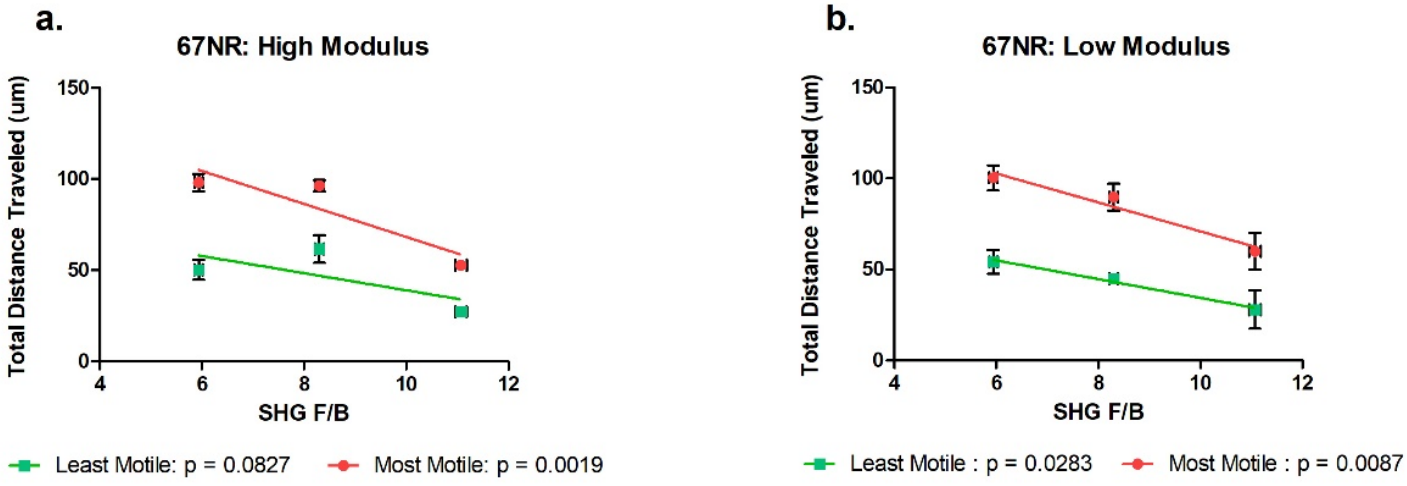

Figure 6

Effect of collagen fiber internal structure, as reported by F/B, and elastic modulus on tumor cell motility of non-metastatic 67NR cells. Data shown as averages ± SEM (n=3). (a) Total distance traveled of the most and least motile 67NR cells on high modulus gels of various F/B. (b) Total distance traveled of the most and least motile 67NR cells on low modulus gels of various F/B. Stated p values represent differences between linear regression slopes and a slope of zero.